Integration of phase change materials in compressed hydrogen gas systems: Modelling and parametric analysis

Mazzucco, Andrea; Rothuizen, Erasmus; Jørgensen, Jens-Erik; Jensen, T.R.; Rokni, Masoud

Published in:
International Journal of Hydrogen Energy

Link to article, DOI:
10.1016/j.ijhydene.2015.09.034

Publication date:
2016

Document Version
Peer reviewed version

International Journal of Hydrogen Energy, Vol. 41, No. 12, 2016, p. 1060-1073

Integration of phase change materials in compressed hydrogen gas systems: modelling and parametric analysis

Andrea Mazzucco[a], Erasmus Rothuizen[a], Jens-Erik Jørgensen[b], T. R. Jensen[c], Masoud Rokni[a]*

[a] Department of Mechanical Engineering
Technical University of Denmark, Nils Koppels Allé 403, DK-2800 Kongens-Lyngby, Denmark
andmaz@mek.dtu.dk; edro@mek.dtu.dk; mr@mek.dtu.dk

[b] Center for Materials Crystallography iNANO and Chemistry Department
University of Aarhus' Langelandsgade 140 8000 Aarhus C, Denmark
jenserik@chem.au.dk

[c] Center for Materials Crystallography iNANO and Chemistry Department
University of Aarhus, Langelandsgade 140 8000 Aarhus C, Denmark
trj@chem.au.dk

Abstract

A dynamic fueling model is built to simulate the fueling process of a hydrogen tank with an integrated passive cooling system. The study investigates the possibility of absorbing a part of the heat of compression in the high latent-heat material during melting, with the aim of saving the monetary and energy resources spent at the refueling station to cool the gas prior to tank filling. This is done while respecting the technical constraint of keeping the walls below the critical temperature of 85 °C to ensure the mechanical stability of the storage system even when the gas is fueled at ambient temperature. Results show that a 10-mm-thick layer of paraffin wax can absorb enough heat to reduce the adiabatic temperature by 20 K when compared to a standard Type IV tank, but its influence on the hydrogen peak temperature that occurs at the end of refueling is modest. The heat transfer from the gas to the phase change material, mainly occurs after the fueling is completed, resulting in a hydrogen peak temperature higher than 85 °C and a lower fueled mass than a gas-cooled system. Such a mass reduction accounts for 12% with respect to the case of a standard tank system fueled at -40 °C. A parametric analysis that embraces the main thermal properties of the heat-absorbing material as well as the major design parameters is here carried out to determine possible solutions. It is found that the improvement of a single thermal property does not provide any significant benefit and that the most effective strategy consists in augmenting the heat transfer area by employing extended surfaces or the encapsulation technique.

Keywords: phase change material; hydrogen storage; hydrogen fueling; dynamic model; heat transfer.

*Corresponding author

1. Introduction

Recent interest has raised for phase change materials (PCMs) as attractive options to store the thermal energy coming from intermittent sources and enable a continuous availability of the stored heat.

Their use provides considerable advantages when compared to technologies that are based on sensible cooling/heating processes. Indeed, great convenience arises from the possibility of using their high energy storage densities to store large amounts of heat in a reduced space, as well as the capability of absorbing and releasing the heat via isothermal heat transfer. These aspects have made PCMs promising candidates for a large variety of applications, including solar energy storage, air conditioning of buildings and spacecrafts, passive cooling of electronics, textiles and fabrics [1]–[9].

A considerably less explored area of study is hydrogen storage. In such a field, research has mainly focused on employing PCMs to absorb the heat that originates during hydrogen fueling in metal hydride tanks for stationary applications [10], [11].

In this study, our interest is to investigate the potential advantages and drawbacks of integrating an adequate PCM into compressed gaseous hydrogen (CHG) storage systems for light duty vehicles. The materials that are used in the walls of commercialized tanks must be maintained below the critical temperature of 85 °C in order to ensure the mechanical stability of the storage system. During fueling the hydrogen temperature rises sharply due mainly to the heat of compression, whereas the inverse Joule-Thomson effect plays a modest role in the temperature increase. In practice, the gas needs to be cooled from the ambient temperature down to -40 °C at the refueling station to prevent the tank walls to reach the critical condition. This procedure ensures that the hydrogen maximum temperature inside the tank never reaches 85 °C during the fueling process, meaning that the mechanical stability of the system is ensured even in presence of non-uniform temperature distribution and local effects as hot spots. However, this system is costly in terms of both energy and capital investment due to the low operation temperatures and the non-conventional technology employed in the hydrogen cooling. Another drawback of the present fueling procedure concerns the lack of dependability that occurs whenever active cooling systems are used. Indeed, even in presence of redundant heat exchangers, possible malfunctioning or failures can threaten the normal operation of the fueling station and hence, the fueling of the vehicles.

The use of integrated passive cooling solutions in the tank is here investigated with the final aim to reduce the cooling demand at the refueling station by absorbing a significant amount of the heat of compression inside the tank and, at the same time, keeping the walls below the critical temperature.

2. Phase change materials

The classification of phase change materials depends on the categorization criteria, which include the final application, chemical composition, range for latent heat or melting temperature values and cost. Table 1 presents a list of PCMs that embrace paraffins, fatty acids, hydrated salts, organic and inorganic compounds for which at least three thermophysical properties amongst melting temperature, heat of fusion, thermal conductivity and density have been measured.

Table 1. Some substances with potential use as PCMs. Property measurements at 1 bar.

Compound	Melting temperature [°C]	Heat of fusion [kJ/kg]	Thermal conductivity [W/m·K]	Density [kg/m^3]

Paraffins				
C_{13-24} [12]	22–24	189	0.21 (solid)	760 (liquid at 70 °C)
C_{22-45} [12]	58–60	189	0.21 (solid)	795 (liquid at 70 °C)
n – Hexacosane [13]	56	257	0.21 (solid)	770
n – Heptacosane [13]	59	236	0.21 (solid)	773
Paraffin wax [14], [15]	64	173.6	0.167 (liquid at 63.5 °C)	790 (liquid at 65 °C)
Fatty acids				
Caprylic acid [14], [15]	16	148.5	0.149 (liquid at 38.6 °C)	901 (liquid at 30 °C)
Lauric acid [12], [15]	42–44	178	0.147 (liquid at 50 °C)	862 (liquid at 60 °C)
Myristic acid [12]	54	187	n.a.	861 (liquid at 55 °C)
Palmitic acid [14], [15]	64	185.4	0.162 (liquid at 68.4 °C)	850 (liquid at 65 °C)
Stearic acid [14], [15]	69	202.5	0.172 (liquid at 70 °C)	848 (liquid at 70°C)
Hydrated salts				
$K_2HO_4 \cdot 4H_2O$ [13]	18.5	231	n.a.	1447 (liquid at 20 °C)
$CaCl_2 \cdot 6H_2O$ [13]	29–30	172–192	0.561 (liquid at 61.2 °C)	1562 (liquid at 32 °C)
$Na_2S_2O_3 \cdot 5H_2O$ [12]	48	209	n.a.	1600 (solid)
$Ba(OH)_2 \cdot 8H_2O$ [13]	78	265-280	0.653 (liquid at 87.5 °C)	1937 (liquid at 84 °C)
$Mg(NO_3)_2 \cdot 6H_2O$ [13]	89-90	162-167	0.490 (liquid at 91 °C)	1550 (liquid at 94 °C)
Organics				
Polyglycol E400 [14], [15]	8	99.6	0.187 (liquid at 38.6 °C)	1125 (liquid at 25 °C)
Polyglycol E600 [14], [15]	22	127.2	0.189 (liquid at 38.6 °C)	1126 (liquid at 25 °C)
Polyglycol E6000 [14], [15]	66	190	n.a.	1085 (liquid at 70 °C)
Naphthalene [14], [15]	80	147.7	0.132 (liquid at 83.8 °C)	976 (liquid at 84 °C)
Erythritol [16], [17]	118.0	339.8	0.326 (liquid at 140 °C)	1300 (liquid at 140 °C)
Inorganics				
H_2O [12], [18]	0	333	0.612 (liquid at 20 °C)	998 (liquid at 20 °C)
$CaCl_2 \cdot 6H_2O$ [14], [15]	29	190.8	0.54 (liquid at 38.7 °C)	1562 (liquid at 32 °C)
$Zn(NO_3)_2 \cdot 6H_2O$ [14], [15], [19]	36	146.9	0.464 (liquid at 39.9 °C)	1828 (liquid at 36 °C)
$Na(CH_3COO) \cdot 3H_2O$ [20]–[24]	58	264	n.a.	1450
$Ba(OH)_2 \cdot 8H_2O$ [12], [14], [19], [20], [22]	78	265.7	0.653 (liquid at 85.7 °C)	1937 (liquid at 84 °C)
$MgCl_2 \cdot 6H_2O$ [14], [15], [19], [20]	117	168.6	0.57 (liquid at 120 °C)	1450 (liquid at 120 °C)
KNO_3 [25], [26]	78	266	0.5	2.110
$NaNO_3$ [25], [27]	307	172	0.5	2260
Na_2CO_3 [25]	854	275.7	2	2.533

n.a.: not available.

For more comprehensive lists, the reader is referred to the papers of [1], [13], [28].

The categorization criteria often involve the material properties which are physically correlated and the selection of one of them is not typically independent from the others. However, it is fair to say that

depending on the particular application, the PCM should first be selected based on its melting temperature.

2.1 Phase change materials for hydrogen storage applications

In this study, we are interested in selecting materials whose characteristics are suitable for absorbing the heat generated during hydrogen fueling in storage tanks, and therefore, it is necessary to identify the desired characteristics that match with such an application.

The thermophysical properties requirements for the PCMs that have to be integrated in hydrogen gas storage applications for light duty systems include: high latent heat, high conductivity in both solid and liquid phase and low density in order to limit the extra weight to the storage system. The melting temperature needs to lie in the practical range of operation, which can be considered between 50-60 °C to avoid spontaneous melting in hot climates prior to hydrogen fueling. Melting should occur congruently and the chemical stability as well as the non-reactivity with the tank materials and with the air/hydrogen mixture must be guaranteed at any time. In addition, other characteristics that take into account health, flammability and physical hazards should also be considered. A fundamental aspect that needs to be taken in consideration is tradeoff that arises from operating with high density materials. Indeed, while large densities provide greater thermal storage capacity per unit volume, they also increase the extra weight added to the system. This aspect is typically of secondary importance for stationary applications, whereas it might be crucial for onboard storage systems to be employed in light duty vehicles, and therefore it will be investigated in the parametric analysis. Finally, low cost material solutions should be preferred [1].

From Table 1 hydrated salts appear to be attractive candidates for gas cooling in hydrogen tanks due to their high volumetric thermal capacities and relatively large thermal conductivities (0.5 $W \cdot m^{-1} \cdot K^{-1}$). They are also generally cheaper when compared to paraffin waxes. However, the negative aspects concerning phase segregation and subcooling make these materials not suitable for applications where the PCM must undergo multiple phase-change cycles in a closed volume, as it occurs in the system investigated in this study. An extensive research is trying to solve these issues by exploring solutions that include the addition of thickening and nucleating agents or the extra water principle [29]. Unfortunately, all these options have the drawback of reducing the conductivity and/or the energy storage density of the compound [1]. In addition, their corrosive nature with metals poses major challenges of compatibility with the tank materials and adequate containment measures as encapsulation are needed to prevent direct contact with the vessel components.

Several studies that aimed at determining the thermal properties of fatty acids have reported that despite the wide range of melting temperatures, these materials generally show low thermal conductivities and modest latent heats [30]–[34]. Their poor thermal properties have prevented their use in commercial systems and limited their applications to property measurements in laboratories.

Among all the PCMs, paraffin waxes appear to be the most attractive materials to be used in hydrogen storage tanks because of their suitable melting temperatures and moderately high latent heats. They are also stable, chemically inert, non-toxic and they do not experience phase segregation during melting. However, pure paraffin waxes are very expensive and it is only advisable to use commercial grade paraffins, which are mixtures of different hydrocarbons obtained from petroleum distillation. It follows that as they are not pure substances, it is more appropriate to refer to a melting temperature range rather than a single melting point to describe the phase change process.

The major drawback of such materials is their poor thermal properties (with thermal conductivities of approximately 0.2 $W \cdot m^{-1} \cdot K^{-1}$), which limit their applications. Different technologies including the addition of metallic fillers, finned tubes, metal and graphite matrix-structures have been investigated with the final aim of augmenting the effective thermal conductivity [35]. The latter solution was proven to be very promising providing an increase in the effective thermal conductivity from 0.24 $W \cdot m^{-1} \cdot K^{-1}$ up to 4–70 $W \cdot m^{-1} \cdot K^{-1}$ for a high porous graphite matrix with 95wt% of paraffin [36].

At the end, it does not seem possible to identify in the literature a single material that possesses all the desirable characteristics and, for what above discussed, a paraffin wax is here selected as the most promising candidate and therefore, it is used in the simulations.

2.2 Encapsulation of phase change materials

Encapsulation is a process that consists in covering the phase change material with a suitable coating or shell material. The main advantages of this technique comprise heat transfer area augmentation, reduced reactivity with the surroundings and containment of the material during phase change.

Thermal and mechanical stability of the PCM are often improved through encapsulation and therefore, these aspects should also be included among the general benefits [37], [38].

Different technologies belong to the encapsulation technique and can be classified with respect to the coating material used, the geometry and the physical principle of containment as well as the size. Plastic and metal are the most used class of materials used to form the containers, which are typically shaped as spheres or tubes/cylinders according to the specific application. The PCM can be held in the containment volume by mechanical confinement, capillary forces or other physical/chemical bonds with the supporting material. Based on size, encapsulated PCMs can be distinguished as macro (for characteristic lengths above 1 mm), micro (between 1 μm and 1 mm) or nano (below 1 μm).

For the application of interest in this study, the heat transfer improvement that can be achieved through encapsulation is an attractive aspect that will be simply explored in the parametric analysis, by varying the heat transfer area for a constant PCM volume.

3. Methods

At first, a computational model that enables to calculate the PCM temperature and provides information on the position of the moving melting layer is developed by means of the effective capacity method [39]. Then, such a model is applied to a 10-mm-thick layer placed at the inner wall of a storage tank, which is filled with high pressure hydrogen. The gas is delivered at practical fueling conditions that are function of the tank type and ambient temperature according to the fueling protocol implemented in the refueling station model, as explained in detail in the next sections. The results are used to evaluate the effect of the PCM on the stored hydrogen mass and profile temperature at the walls for the novel vessel design in comparison with the standard tank solution currently available on the market.

3.1 Phase-change and heat transfer models

The PCM used is a paraffin wax with a melting temperature T_m of 55 °C, latent heat λ of 224.36 kJ/kg and thermal conductivity that varies between k_s = 0.24 $W \cdot m^{-1} \cdot K^{-1}$ for the solid and k_l = 0.18 $W \cdot m^{-1} \cdot K^{-1}$ for the liquid phase. More details on the PCM properties can be found in Ref. [39]. As the physical and thermal properties of the PCM have only been measured in the liquid and solid phases, in

the model they have been linearly interpolated during phase change with respect to the instantaneous temperature value.

The energy balances and heat transfer equations are solved for the hydrogen gas and the wall, which has been discretized by means of the finite volume method in Dymola® environment [40]. In Fig. 1 the discretization concept and the heat transfer flows are presented with attention to the PCM and along with the boundary conditions.

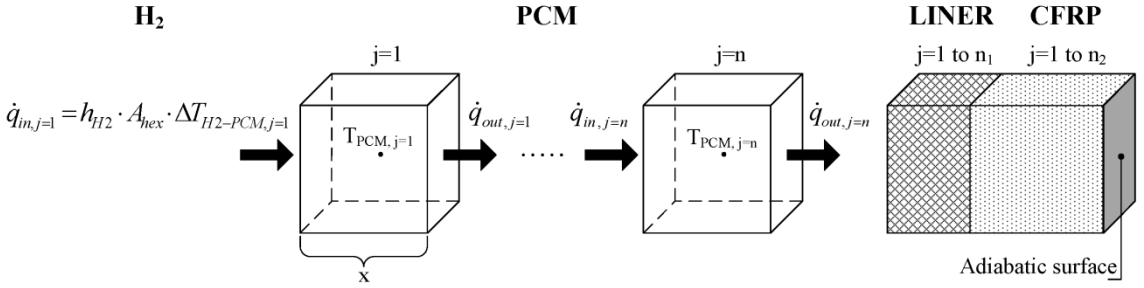

Figure 1. Discretization sketch of the tank walls.

The convection coefficient in the boundary condition at the hydrogen-PCM interface varies between 150-500 $W \cdot m^{-2} \cdot K^{-1}$, as discussed in Ref. [41].

The transient one-dimensional energy balance for each PCM volume reads:

$$\rho \cdot c_p \cdot \frac{\partial T_{PCM}}{\partial t} \cdot (x \cdot A_{hex}) = \dot{q} \ \ [\mathrm{W}] \tag{1}$$

where ρ is the density, T_{PCM} is the temperature calculated at the volume center point, x is the discretization step (defined on a path parallel to the heat flow), A_{hex} is the heat transfer area and c_p is the specific heat capacity computed by means of the effective capacity method for a melting range of 52-56 °C, representative of the asymmetrical triangular delta-function that provided the highest agreement between computational and experimental data as described in [39].

The overall heat transfer rate $\dot{q}$ for each control volume accounts for both the heat that flows in, $\dot{q}_{in}$ and out, $\dot{q}_{out}$ which are function of the thermal resistance R_{th}, calculated along x, and the temperature difference between the center points of the PCM volumes, as presented in Eqs. (2) to (5):

$$\dot{q} = \dot{q}_{in} + \dot{q}_{out} \ [\mathrm{W}] \tag{2}$$

$$\dot{q}_{in} = (T_{in} - T_{PCM}) / R_{th} \ [\mathrm{W}] \tag{3}$$

$$\dot{q}_{out} = (T_{out} - T_{PCM}) / R_{th} \ [\mathrm{W}] \tag{4}$$

$$R_{th} = \frac{x}{A_{hex} \cdot k_{PCM}} \ [\mathrm{K \cdot W^{-1}}] \tag{5}$$

The heat transfer model accounts for the conduction in the solid phase, natural convection in the liquid phase and their combination during melting. This is done via the definition of an effective thermal conductivity k_{PCM} that varies accordingly to the procedure reported below:

$$
\begin{aligned}
&\textit{if } T_{PCM} < T_m - \delta_1 \\
&\quad k_{PCM} = k_s \\
&\textit{if } \; T_m - \delta_1 \le T_{PCM} \le T_m \\
&\quad k_{PCM} = k_s + (k_m - k_s) \cdot (T_{PCM} - (T_m - \delta_1))/(\delta_1) \\
&\textit{if } \; T_m < T_{PCM} < T_m + \delta_2 \\
&\quad k_{PCM} = \mathrm{k_m} + ((\mathrm{k_l} \cdot \mathrm{k_{r2}}) - \mathrm{k_m}) \cdot (\mathrm{T_{PCM}} - \mathrm{T_m})/\delta_2; \\
&\textit{if } T_{PCM} \ge T_m + \delta_2 \\
&\quad k_{PCM} = k_l \cdot k_{r1}
\end{aligned}
$$

with,

$$\delta_1 = 3 \text{ [K] or [°C]} \tag{6a}$$

$$\delta_2 = 1 \text{ [K] or [°C]} \tag{6b}$$

$$\mathrm{k_m} = \mathrm{k_s} + (\mathrm{k_l} \cdot \mathrm{k_{r2}} - \mathrm{k_s}) \cdot \delta_1/(\delta_2 + \delta_1); \; [\mathrm{W \cdot m^{-1} \cdot K^{-1}}] \tag{7}$$

where δ_1 and δ_2 represent the values assumed by the asymmetrical delta-function during phase change, k_m is the linearly interpolated thermal conductivity calculated at T_m, whereas k_{r1} and k_{r2} are the ratio between the effective conductivity that accounts for natural convection and the thermal conductivity of the liquid defined accordingly to Ref. [42]. For the geometry of interest (i.e. annular region between long horizontal concentric cylinders with heated inner surface), the general expression of such a ratio reads:

$$\mathrm{k_r} = \frac{\mathrm{k_{PCM}}}{\mathrm{k_l}} = 0.386 \cdot (\mathrm{P_r}/(0.861 + \mathrm{P_r}))^{1/4} \cdot \mathrm{Ra}^{1/4} \; [-] \tag{8}$$

This correlation is valid for $0.7 \le \mathrm{P_r} \le 6000$ and $\mathrm{Ra} \le 10^7$. As the minimum heat transfer cannot fall below the conduction limit, the effective thermal conductivity is imposed equal to k_l when the value predicted by Eq. (8) is less than unity.

The Rayleigh number in Eq. (8) is computed with respect to the relevant temperature difference for k_{r1} and k_{r2}. For the former, this difference considers the time-dependent temperatures of the volumes at the two extremities of the PCM layer (i.e. at j=1 and j=n, see Fig. 1), whereas for the latter it refers to the inner volume's central-point temperature (i.e. at j=1, see Fig. 1) and the upper temperature in the melting range, $T_m + \delta_2$, as a reasonable approximation.

3.2 Hydrogen fueling model

In this section, only the tank design and the working principle of the model that describes the operation of the fictitious refueling station are explained, as the thermodynamic and heat transfer models employed in the tank are described in detail in Ref. [41], [43]. A simplified sketch representing the dynamic fueling model implemented in Dymola® is presented in Fig. 2.

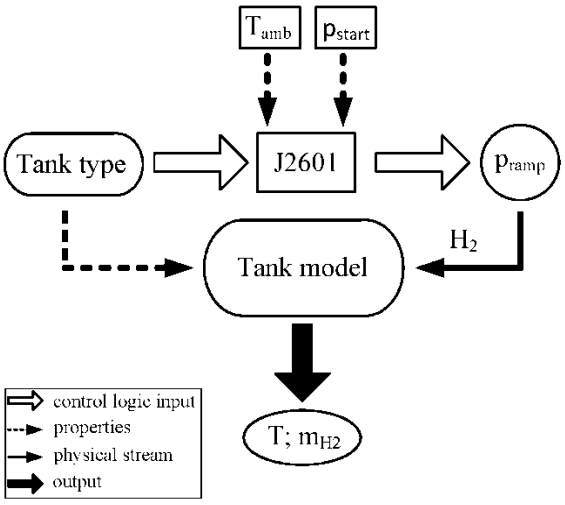

Figure 2. Sketch of the computational fueling model.

From such a figure, it can be observed that the tank type (e.g. Type III, Type IV) with its physical properties and initial internal pressure (i.e. p_{start}), and the ambient temperature (i.e T_{amb}) constitute the main inputs that are passed to the J2601 model component that selects the hydrogen charging pressure (350 or 700 bar) and its pressure ramp according to the refueling protocol SAE J2601 [44].
The high pressure gas is then fueled into the tank model component where the thermal model presented in the previous sub-section is implemented. Such a component computes the temperature rise that occurs during hydrogen fueling and calculates the heat that is transferred to the PCM thickness and through it to the liner and carbon fiber that constitute the tank walls.

The main outputs of the model include the hydrogen temperature, the temperature profile in the PCM layer and in the walls at different locations, as well as the stored hydrogen mass (i.e. m_{H2}).
In the model, it is possible to select the boundary condition for the outer surface of the tank as adiabatic or alternatively calculate the heat losses due to the natural convection in the ambient air. For the scope of this study, the former option provides a more conservative approach and it is therefore employed to obtain the results presented in the following section.

3.3. Tank design

In Fig. 3 the dimensions of the Type IV tank considered in this study are reported, while the liner and carbon fiber properties are given in Ref. [45]. The inner volume is approximately 126 L, which is a realistic size for a practical storage system to be used in a fuel cell vehicle (FCV).

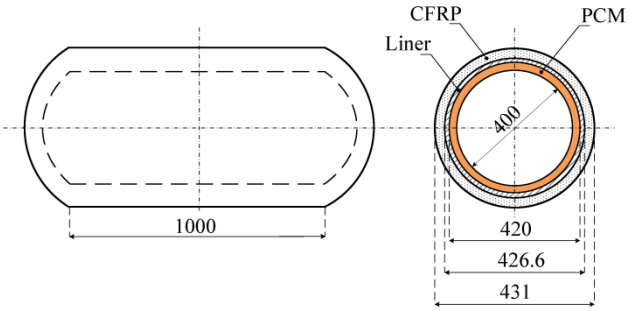

Figure 3. Type IV tank longitudinal and transversal sections. All dimensions are in mm.

In practice, a thin aluminum layer can be used to keep the phase change material in place and prevent it to flow to the bottom of the tank during melting. The thickness of the confinement layer is hereby assumed to be small enough to have a negligible influence on the total tank's volume and weight as well as on the heat transfer process. Further studies should focus on the selection of the most adequate technology to confine the PCM and the analysis of its mechanical stresses during periodical fueling. These aspects are out of the scope of the present work which aims at addressing the potential convenience of the proposed technology from an energy-saving perspective.
In Table 2, an immediate comparison between the overall size and weight of the two tanks is given. The two tanks are compared with respect to the same inner volume.

Table 2. Type IV tank and novel design: size and weight.

Case	V_{tot} [L]	m_{tank} [kg]	m_{PCM} [kg]
Standard Type IV	160	45.6	/
Type IV with PCM	174 (+9%)	57.75 (+27%)	10

When a 10-mm-thick layer is inserted on the inner wall, the overall tank volume increases by 9%, and it's mass by 27%. Such a mass increase is mainly due to the PCM, which accounts for 10 kg of the extra 12 kg added to the tank. The rest is due to the larger masses of the liner and carbon fiber reinforced polymer (CFRP) that result from keeping the same thickness at larger radii. At the end, while the difference in volume is modest, the mass increase appears quite significant. However, the extra weight added to the system is relatively negligible when the comparison is made with respect to the overall FCV mass.

4. Results

4.1 Thickness analysis

The discretization of the PCM layer allows identifying the solid/liquid front as it moves towards the wall of the tank at greater times, making possible to determine whether exists a portion of the PCM material that does not undergo the phase change and hence provides mainly an insulation effect rather than heat absorption. In case this occurs, it should be investigated whether it is possible to decrease the

PCM thickness, reducing the extra mass and volume added to the system, while maintaining the same thermal performance. Different thicknesses are here investigated, ranging from 2.5 mm to 50 mm. Such a range also includes the nominal condition presented in Fig. 3, which considers a 10-mm-thick layer.

Three different cases can be identified by investigating the adiabatic temperature T_{adiab}:

1) $T_{adiab} > T_m + \delta_2$
2) $T_m - \delta_1 < T_{adiab} < T_m + \delta_2$
3) $T_{adiab} < T_m - \delta_1$

For case 1) all the PCM melts and in stationary conditions the material is in the liquid form.
This is in principle the most favorable scenario, as it ensures that the entire mass of PCM has experienced the phase change and absorbed the energy that corresponds to its latent heat.
Case 2) implies that the material is partially melted; hence its latent heat has not been entirely exploited. Case 3) comprises equilibrium temperatures below the melting range, indicating that only the sensible heat has been exchanged and hence, considering the poor thermal properties of the paraffin wax, the PCM behaves as an insulation thickness during the phase change process.
In Fig. 4 the melting range is represented as a grey area. The results are presented for a location $x_{½}$ that corresponds to the half-thickness of the corresponding layer. In order to give the reader direct information of the total thickness' value, $x_{½}$ is expressed as the entire thickness divided by two in the figure's legend.

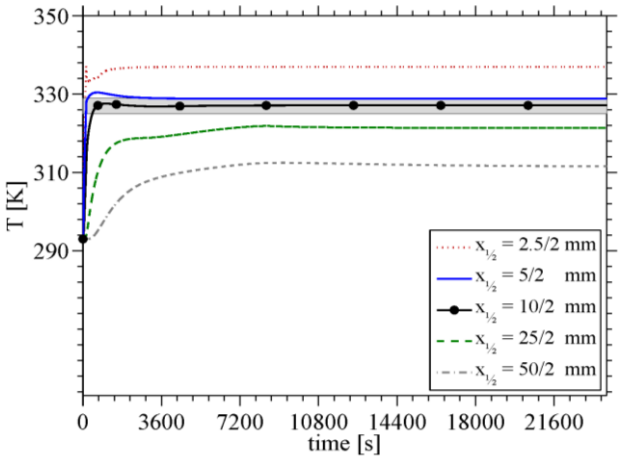

Figure 4. Temperature profiles at the half of the PCM layer for different thicknesses values.

As expected, for thicker layers the adiabatic temperature decreases and the system reaches the stationary conditions at larger times. For a thickness of 5 mm T_{adiab} lies on the upper value of the melting range and therefore, this condition belongs to case 1). It follows that layers below or equal to 5 mm will ensure a complete melting of the PCM thickness, whereas above such a value T_{adiab} will belong to case 2) or case 3). It can be observed that for the nominal thickness of 10 mm, the temperature at stationary conditions assumes the value of 326 K which lies within the melting range. As a result, case 2) occurs and the actual cooling does not take advantage of the entire latent heat

available. For layers of 25 and 50 mm, T_{adiab} settles at approximately 317 and 301 K respectively, and the material only exchanges sensible heat. The large thermal capacity of the PCM is unused.

As only the adiabatic temperatures have been discussed here, the comparison among different thicknesses has been made with respect to large times, when the system reaches stationary conditions. However, in order to further investigate the effect of the thickness on the system's cooling performance, a dynamic refueling analysis for different layers is presented in the parametric analysis section.

4.2 Refueling analysis and energy saving

A comparison in results between a standard Type IV tank and the design with integrated PCM is here provided. The temperatures in the plots refer to the location corresponding to half of the thickness of each wall layer.

In Fig. 5 the results obtained under the assumptions of adiabatic outer wall and absence of hydrogen cooling at the fueling station are shown. The gas is filled at the ambient temperature of 20 °C, which is the system's equilibrium temperature before the fueling takes place, and rapidly heats up due to the compression into the tank. With a pressure ramp of 282 bar/min, the fueling is completed in approximately 150 s, and the gas reaches its peak temperature around 390 K. Being the outer tank wall adiabatic, the heat can only be transferred from the gas to the surrounding walls and the system tends to thermal equilibrium.

In Fig. 5a, where the results for a standard Type IV tank are presented, the adiabatic temperature is around 74 °C and the thermal equilibrium is reached at 3300 s.

During fueling, the gas thermal convection coefficient is set to 150 $W \cdot m^{-2} \cdot K^{-1}$ (see Ref. [45]) and the plastic liner experiences higher heat rates, whereas, when the filling process is completed, the convection coefficient drops to 50 $W \cdot m^{-2} \cdot K^{-1}$ and the liner undergoes an abrupt decrease in temperature, because more heat is transferred outward to the wall, and then it heats up again.

Under these conditions, the adiabatic temperature is below the critical value for both the liner and CFRP. However, the presence of hot spots where the local temperature might be greater than 85 °C should not be excluded, with the result that the mechanical stability of the tank might be damaged.

In Fig. 5b the temperature results that refer to the novel Type IV tank with PCM material are presented.

The system reaches the thermal equilibrium at a temperature around 54 °C, which is approximately 20 °C lower than for the standard tank case. It follows that, the phase change material succeeds in absorbing a significant amount of the heat of compression, keeping the walls considerably below the critical temperature at any time. However, as in the previous case, the hydrogen temperature seems affected by the heat transfer to the walls only after the filling process is completed and large times are required to reduce the gas temperature below 85 °C and later reach the thermal equilibrium. By comparing Fig. 5b with Fig. 5a, it can be observed that the peak temperature is reduced by only 2 K when the phase change material is inserted, meaning that the heat transfer rates are not high enough to effectively exchange the heat of compression during fueling. Indeed, the high thermal resistances at the hydrogen/gas interface, as well as the poor thermal properties of the paraffin wax, limit the gas cooling and slow down the heat transfer process.

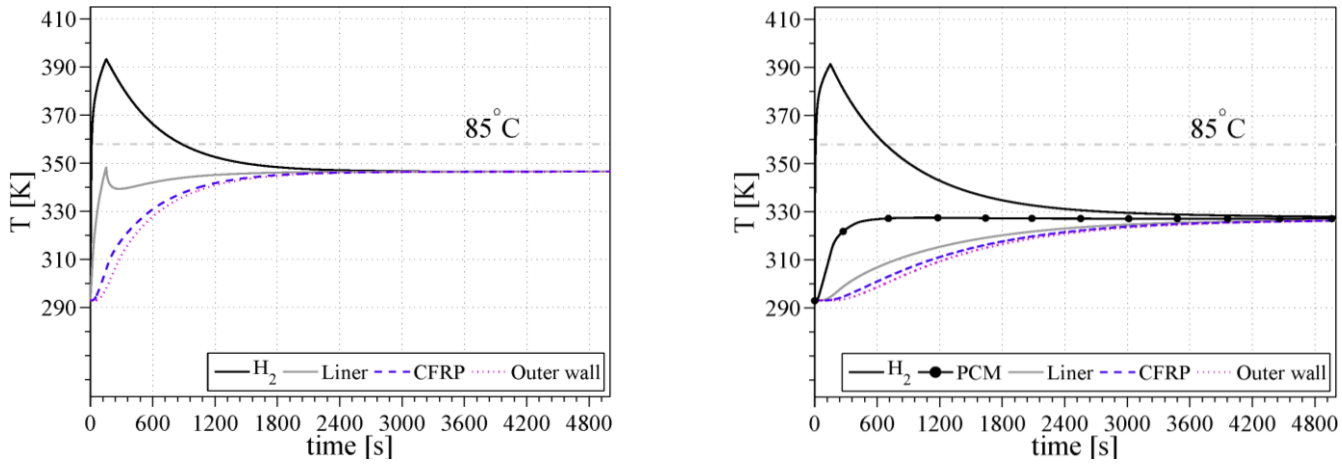

(a) (b)

Figure 5. Temperature profiles for a standard Type IV tank (a) and for a Type IV tank with integrated PCM at the inner wall (b). No hydrogen cooling at the station.

At the end, two main conclusions can be drawn. First, the presence of hot spots at the walls cannot be entirely excluded, although the insertion of the PCM layer makes such a situation quite unlikely; second, the gas density during fueling is the same for the two tanks, resulting in the same overall mass that is fueled into the storage system. With respect to the latter assertion and even if it is assumed that no hot spots would result in practice, the present novel design cannot provide the same storage performances of a regular CHG system, where the hydrogen is cooled prior to filling.

This can be observed in Fig. 6a where the hydrogen mass inside the tank is presented at different gas inlet temperatures. At time zero, the gas inside the tank is at the initial conditions of 20 bar and 20 °C and the resulting initial hydrogen mass is 0.2 kg. When refueling starts, the gas mass increases until the target charging pressure is reached at 150 s. Then, the inlet valve closes and the stored mass remains constant. For the same storage volume, the overall fueled mass is reduced from 4.67 kg, when hydrogen is filled at -40 °C, to 4.17 kg in absence of gas cooling. This corresponds to a decrease by 12% in the storage capacity of the system.

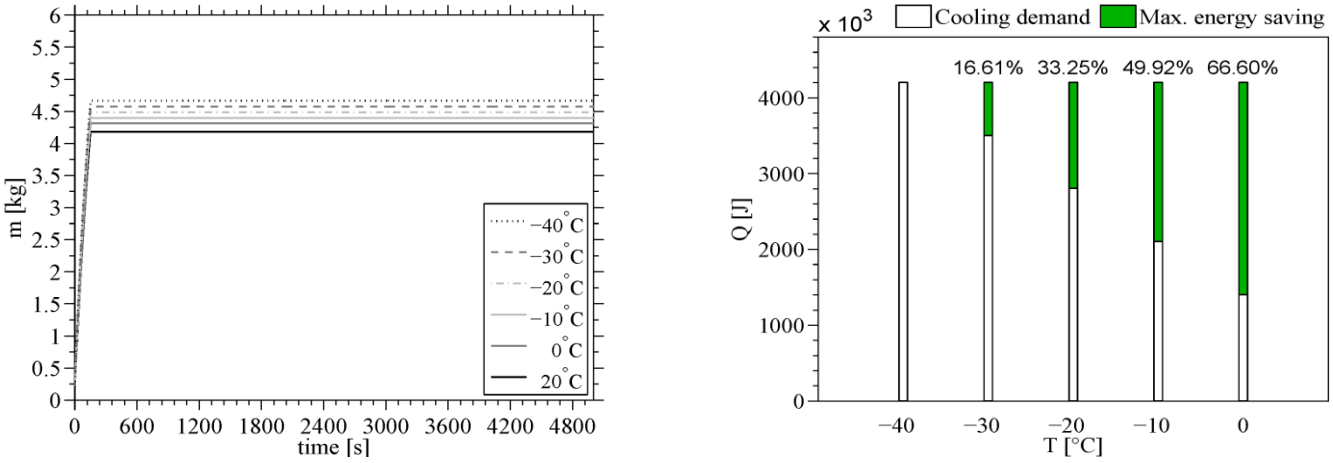

(a) (b)

Figure 6. Hydrogen mass fueled into the tank for different inlet temperatures (a); Cooling demand per refueling at the refueling station and relative maximum energy saving with respect to an inlet gas temperature of -40 °C (b).

Ideally, the novel tank design should guarantee the mechanical stability even in absence of gas cooling and store the same amount of hydrogen as a regular gas-cooled system. If this could be realized, the only drawbacks would be the larger weight and volume, whereas the benefits would include the energy saving and the heat exchanger size-reduction/removal at the refueling station, as well as the increase in the filling process reliability.

In Fig. 6b the cooling energy per refueling that is needed at the refueling station is presented for different temperatures at the tank inlet along with the energy saving calculated with respect to the standard cooling case (i.e. T_{H2} = -40 °C). The reduction in cooling demand is nearly linear with the charging temperature, ranging approximately from 16.6% to 66.6% when the inlet gas temperature is increased from -40 °C to -30 °C and 0 °C respectively. As in the present study the COP and its dependency upon temperature are unknown for the actual refrigeration system in use at the refueling station, it is hereby assumed that the energy savings coincide with the reduction in cooling demand. This corresponds to having a refrigeration system with a unitary COP and thus the obtained energy savings in Fig. 6b are to be intended as maximum values. Such an assumption seems not to be far from reality, if we consider that a COP of approximately 1.1 was recently estimated for a refrigeration system operating at the same ambient temperature considered in this work (i.e. 20 °C) and for a final hydrogen temperature of -40 °C [46]. In practice, when detailed information on the cooling performance is available, it is possible to calculate the real energy savings by dividing their maximum values by the actual COP.

Although from an economic perspective the most favorable case occurs in absence of gas cooling, temperatures around -10 °C allow the use of heat exchangers normally employed in the refrigeration industry, resulting in a considerable cost reduction when compared to non-conventional cooling systems. However, in order to exploit the complete potential of this solution and realize a storage system that is attractive on the market, the tank should enable the same storage performance as the

current technology at inlet gas temperatures greater than -40 °C. In order to achieve such an objective, the heat transfer from the gas to the phase change material must be enhanced and, at the same time, the PCM physical properties should be carefully tailored.

4.3 Parametric analysis

Different parameters that are expected to control the heat transfer process are varied to investigate their influence on the hydrogen temperature evolution. These parameters include the main PCM's thermal properties, thickness and the heat transfer area.

The hydrogen convection coefficient is not varied in the present analysis as the thermal resistance is low compared to the PCM resistance and therefore, no considerable effects on the gas temperature are expected to occur by its augmentation.

In addition, the hydrogen convection coefficient is determined by the refueling conditions and the resulting turbulence inside the tank and hence is fixed for a given design.

4.3.1 PCM properties

In this section, the effect that the main physical properties have on the hydrogen peak temperature is investigated. The main goal is to determine whether it is possible to reduce the gas temperature at the end of refueling by individually improving the thermal properties of the PCM.

The comparison on the gas temperature during filling is presented in Fig. 7 for different values of thermal conductivity, specific heat capacity, density and latent heat of phase change. It must be noticed that the variation ranges for such properties comprise upper values that are non-practical for conventional materials. This choice has been made to obtain a broad view on the extent to which the gas temperature is dependent upon a large variation in the main thermal properties of the PCM.

In Fig. 7a the thermal conductivities for solid and liquid phases are increased from the nominal conditions by a factor up to 10^3. Different strategies can be employed to enhance the thermal conductivity, as the use of a PCM with favorable thermal properties, enhancing the heat transfer by forming PCM stable composites with a highly conductive material, as well as inserting the PCM in a metallic structure (e.g. aluminum foam) [47], [48]. Results show that only modest reductions in the peak temperature occur for such a wide variation range. The maximum hydrogen temperature decreases by only 2 K when the conductivity is doubled and by 4 K when it is augmented by a factor of 10. A more significant reduction can be observed when the conductivities are of the same magnitude as the hydrogen convection coefficient. The gas temperature at the end of fueling reaches a maximum value of 382 K, which is approximately 10 K less than the value obtained at nominal conditions.

Further increases in conductivity only have a negligible effect and the gas temperature curves differ by less than 1 K when the multiplying factor for k_0 increases from 10^2 to 10^3. As the dominating thermal resistance has now become the convection one on the hydrogen side in order to additionally augment the heat transfer, the thermal resistances must be reduced together.

Fig. 7b shows a negligible dependency of the gas temperature upon the latent heat at any time of the filling process as well as after the refueling is completed. In particular, the peak temperature experiences a negligible reduction between the nominal conditions and the maximum latent heat value in the range. This occurs because, although greater latent heats increase the thermal capacity of the system during phase change, the poor thermal properties limit the heat transfer rates preventing the entire PCM mass to undergo the phase change in the short time of the filling process. As a result, the effect of larger latent heats is more important after the refueling is completed, where the divergence of

the temperature curves is more evident, leading to lower temperatures at thermal equilibrium. However, the adiabatic temperature remains approximately constant and a negligible reduction of nearly 2 K occurs for an increase in λ by 10^2 from the nominal conditions. The reason is that at present conditions and for the current design, the lowest adiabatic temperature that the system can reach corresponds to the lowest value in the melting range (i.e. 52 °C) at which the temperature curve for the PCM tends to flatten until the phase change is completed. As for λ_0 the temperature at equilibrium already lies in the melting range and corresponds to 54 °C, it is not possible to decrease T_{adiab} further than 2 K even at large λ. Smaller thicknesses that would lead to higher equilibrium temperatures would leave more room for T_{adiab} reduction at large latent heats.

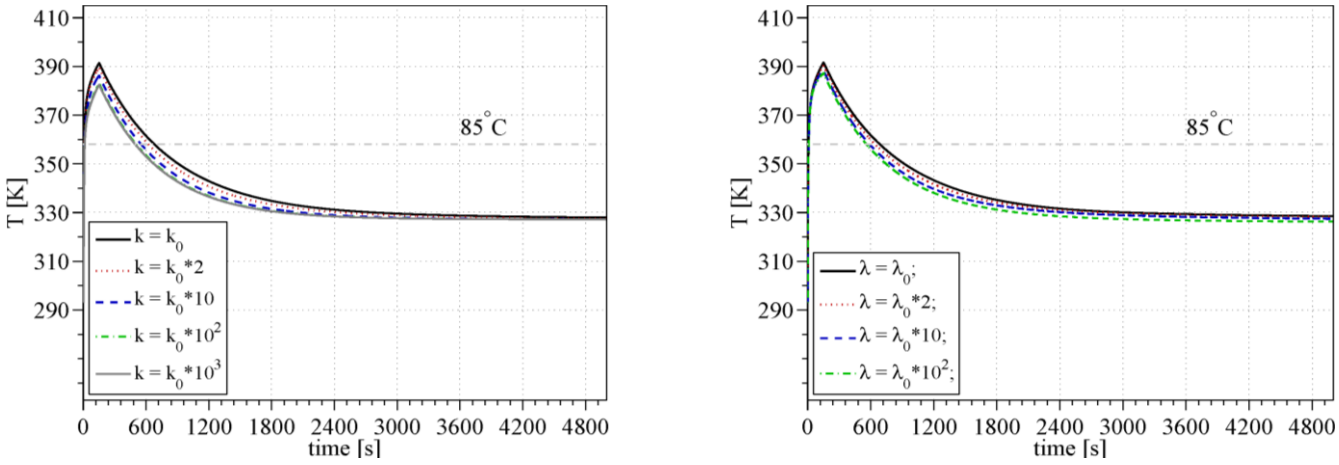

(a) (b)

Figure 7. Hydrogen temperature evolution during fueling for different values of PCM's thermal conductivity (a) and latent heat (b).

In Fig. 8a the gas temperature during fueling is shown for different specific heat capacity values, ranging from the nominal conditions to a value increased by a factor of 10^2.

As it was found in the conductivity analysis, the peak temperature only presents a poor dependency upon c_p. Indeed, the main effect of using a PCM with greater thermal capacities consists in increasing the overall heat that can be absorbed within the phase change material. This can be observed by comparing the adiabatic temperatures obtained for the different c_p values. Doubling the heat capacity only reduces T_{adiab} by 2 K, while for specific heat capacities augmented by a factor of 10 and 10^2, the adiabatic temperature drops by 21 K and 31 K respectively.

On the other hand, the maximum gas temperature reduces by only 1.5 K, 5 K and 13 K respectively, in the same range of variation for c_p.

The same conclusions can be drawn from Fig. 8b, where the dependency of gas temperature upon the PCM density replicates the trend observed in Fig. 8a. This is valid for both the gas maximum and adiabatic temperatures. As for the c_p augmentation, an increase in the PCM density provides a greater

thermal capacity for the heat-absorbing system and hence, a lower temperature at equilibrium, but does not affect much the rate at which the heat transfer occurs.
It should be remembered that the upper limit in the density range is non-practical and that the modest benefit in peak temperature reduction that is gained at such density value is overcompensated by the corresponding increase in the system's mass, which would increase by 10^2 kg.

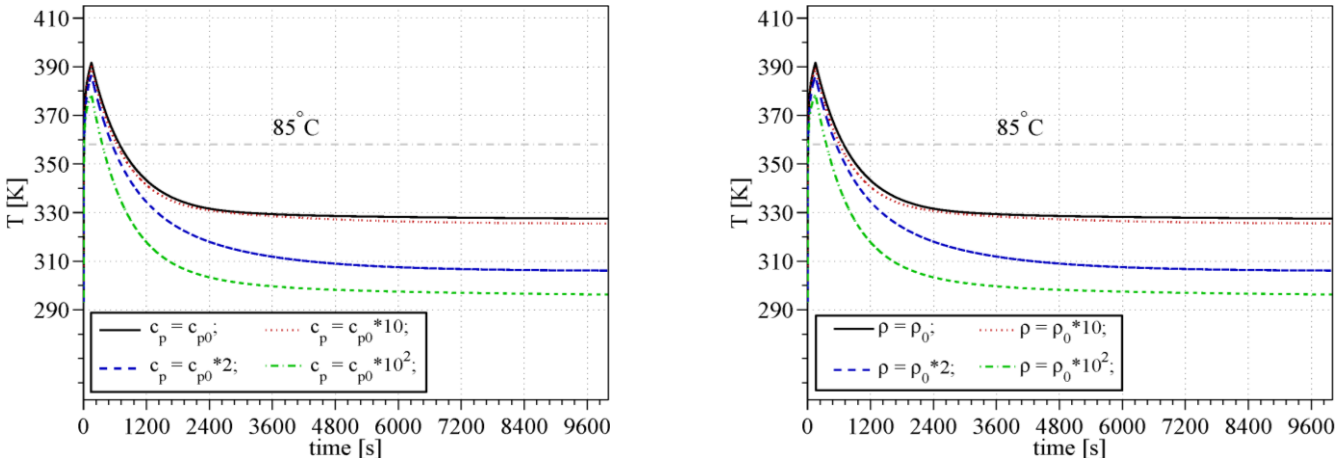

Figure 8. Hydrogen temperature evolution during fueling for different values of PCM's specific heat capacity (a) and density (b).

At the end, it appears that it is not possible to identify a significant dependency of the peak temperature upon a single thermal property of the PCM. For a given design, this result suggests that a combination of different properties values and other parameters should be investigated.

4.3.2 PCM thickness

In Fig. 9 the evolution of the hydrogen temperature over time is shown for different PCM thicknesses. In Fig. 9a it can be observed that the main effect of operating at thicker layers is the reduction of T_{adiab}, whereas the peak temperature appears unvaried. The former outcome has been already pointed out in Fig. 4 with respect to the PCM temperature at a location corresponding to half thickness of each layer. Stationary conditions occur at larger times as the thickness increases, ranging approximately from 3600 s to 23760 s for a layer of 2.5 mm and 50 mm respectively. In addition, it can be noticed that for the first 9360 s the temperature profiles are nearly overlapping for thicknesses of 5 mm and above. In such a time span, stationary conditions are not reached for the PCM located at more than 10 mm which starts melting at 9360 s, participating significantly to the heat absorption and producing a further decrease in temperature.
Fig. 9b presents a zoomed-in view of the previous figure at the end of refueling, for a better comparison among the peak temperatures.

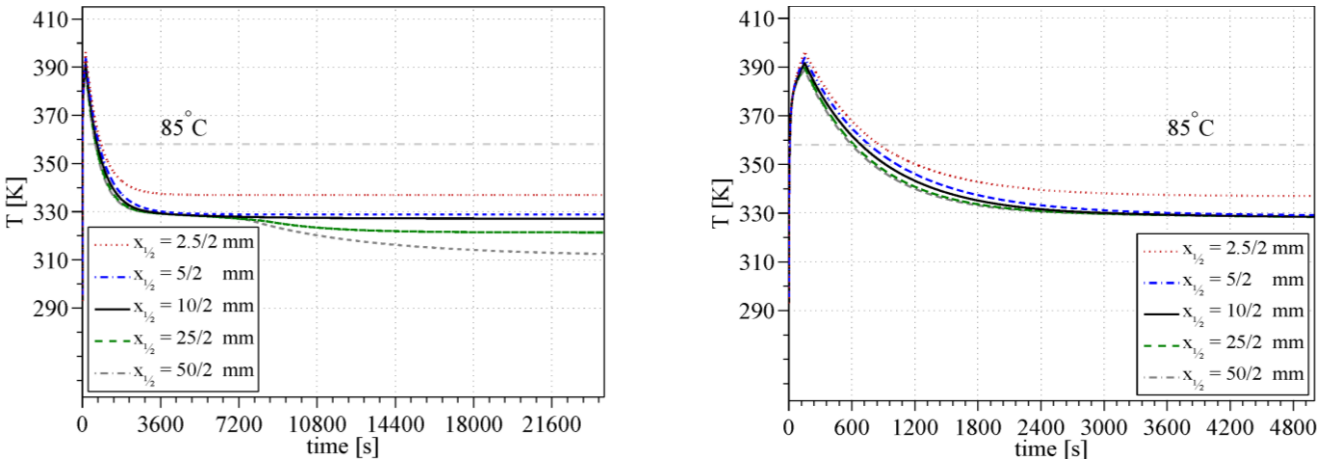

Figure 9. Hydrogen temperature evolution during fueling for different values of PCM's thickness: extended simulation time (a) and zoomed-in view of the peak-temperatures (b).

Such a figure points out the negligible effect of larger thicknesses on the maximum gas temperature. This is due to the poor heat transfer rate at the hydrogen/gas interface, resulting in a decrease by 7 K when the thickness is increased from 2.5 mm to 50 mm. This temperature reduction is more important for layers up to 25 mm, whereas is negligible at larger thicknesses.

At the end, when comparing the tanks with 10 and 5 mm layers, the difference between adiabatic and peak temperatures is modest and hence, the cooling performance can be considered nearly the same. Similar conclusions can be drawn for the amount of hydrogen when considering the two different thicknesses of the layer. The only actual benefit that arises from operating with a 5 mm thick layer is the decrease in the overall system's volume and mass from 174 L and 57.75 kg to 166 L and 51.6 kg respectively. The latter values correspond to an increase by 3.6% in volume and 13.2% in mass with respect to the standard tank case presented in Table 2.

4.3.3 Heat transfer area enhancement

Solutions to augment the heat transfer area include extended surfaces and PCM encapsulation in the liner lattice [37]. The former method only influences the heat transfer area at the hydrogen/PCM interface (A_{in}), whereas the latter affects the entire PCM mass. In the present analysis the computational model is modified to account for both cases by allowing a manual entry of the inner surface area or the heat transfer area (A_{in} and/or A_{hex}) values, without changing the PCM volume and mass. The tank dimensions are kept the same, whereas the heat transfer area is redefined as an input to establish whether it is a limiting parameter for the heat transfer process in the present design. This simplified procedure is based on the assumption that, for the purposes of the heat transfer process, the main effect of extended surfaces and encapsulation lies in the heat transfer area augmentation.

In Fig. 10 the effect of A_{in} and A_{hex} on the hydrogen temperature is shown. The adiabatic temperature remains obviously unchanged as the heat transfer area affects the heat rate and not the heat capacity of the PCM, but larger heat transfer areas make the stationary conditions occur at shorter times.

In Fig. 10a, it can be observed that modest variations in A_{in} provide considerable reductions in the peak temperature. When this area is doubled from the nominal conditions, the maximum hydrogen temperature decreases by 10 K, providing a cooling effect more important than any other parameters investigated above in the same variation range. This suggests that the limiting factor for the heat transfer process in the current design is the reduced area at the hydrogen/PCM interface. The influence on the gas temperature is decreased for larger values of A_{in}, as the poor thermal properties of the heat-absorbing material delay the heat transfer, preventing significant heat absorptions to take place at the end of refueling. As a result, the maximum temperature reduces by only 21 K when A_{in} increases tenfold. Solutions for this involve the enhancement of the heat transfer rate in the PCM, which can be achieved by enlarging the heat transfer area via encapsulation and/or improving the thermal conductivity.

The former option is presented in Fig. 10b, where both the heat transfer area at the hydrogen/PCM interface and of the PCM are augmented at constant volume and mass. The benefit of encapsulation is modest for relatively small increases in the heat transfer area, accounting for a further reduction by approximately 4 K at doubled A_{hex} values. On the other hand, when A_{hex} is increased tenfold, the PCM's thermal resistance is reduced by the same magnitude, enabling significant heat transfer rates and resulting in a considerable decrease in the hydrogen temperature at the end of refueling. Such a reduction accounts for 44 K with respect to the nominal conditions, pointing out the notable effect of operating at lower PCM's thermal resistances for augmented heat transfer areas at the gas interface. What is more important is that the peak temperature is now reduced below the critical value for the mechanical stability of the tank walls. This forestalls the presence of hot spots at the walls and provides higher gas densities at the end of the filling process, resulting in larger hydrogen masses stored in the tank. The overall fueled mass is now 4.52 kg, which accounts for a reduction by 3.3% with respect to the target value obtained for the standard tank case, where the gas is cooled to -40 °C to tank fueling.

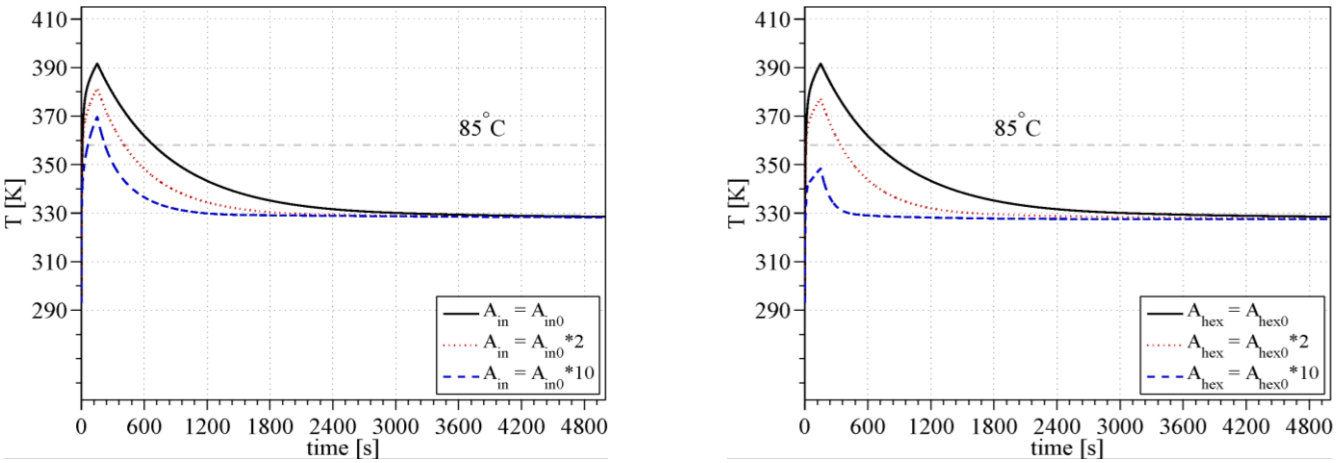

(a) (b)

Figure 10. Hydrogen temperature evolution during fueling for different values of the heat transfer area: at the hydrogen/PCM interface only (a) and for both the hydrogen/PCM interface and the entire PCM layer (b).

At the end it should be stressed, that similar results can be achieved by augmenting the thermal conductivity, as mentioned above. This can be seen in Fig. 11 where a comparison between encapsulation and conductivity enhancement at large A_{in} values is proposed. The temperature trend is nearly the same, differing only in correspondence of the end of refueling, where the curves diverge, leading to a difference in the peak values by approximately 3 K. Such a difference is due to the non-linear influence that the effective thermal conductivity has on the thermal resistance in presence of natural convection.

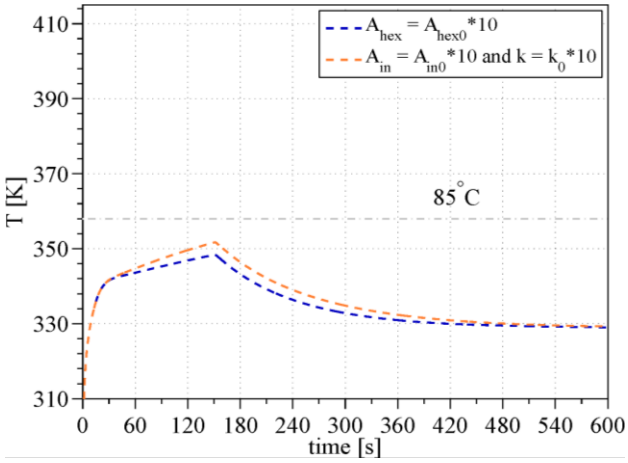

Figure 11. Comparison between encapsulation strategy and thermal conductivity enhancement for large heat transfer areas at the hydrogen/PCM interface. Zoomed-in view, detail of the peak temperature.

5. Conclusion

In order to reduce the cooling demand at the refueling station, a tank with an integrated phase change material is hereby proposed to absorb the heat of compression released during hydrogen fueling. In addition to the energy saving, the novel tank design can improve the economy and the reliability of the fueling process, due to a reduction in the investment cost of the heat exchanger at the refueling station and to the replacement of an active cooling system with a passive one.

Two tank designs are here considered for comparison in absence of hydrogen-cooling at the refueling station: a standard Type IV tank and the novel tank design with a 10-mm-thick layer of PCM in the inner volume. Results show that the integration of the PCM reduces the system's adiabatic temperature from 74 °C to 53 °C when compared to the standard case, but due to the modest heat transfer rates at the hydrogen/PCM interface and in the PCM thickness, the hydrogen peak temperature is essentially independent from the PCM insertion. The maximum temperature reaches values above the critical limit of 85 °C and thus the presence of hot spots that can damage the mechanical stability of the walls cannot be forestalled. The high gas temperatures that occur during fueling cause the fueled hydrogen mass to reduce by 12% with respect to the standard case. A parametric analysis is carried out

to solve this issue by determining the influence of the maximum gas temperature upon the PCM's main thermal properties, thickness and area of heat transfer. The material's thermal properties and thickness were found to only have a modest effect on the hydrogen temperature during refueling, when varied singularly. The reward strategy that is identified consists in a heat transfer improvement by surface augmentation or combined enhancements of the heat transfer area at the hydrogen/PCM interface and PCM's thermal conductivity.

The encapsulation technique can provide sufficiently high surface enlargements to reduce the peak temperature below the critical limit and eliminate the risk of hot spots at the tank walls. In addition, the hydrogen stored mass becomes comparable with the values obtained for the standard case. As an example, when the encapsulation method increases tenfold the heat transfer area for the current design, the maximum gas temperature is reduced from 118 °C to approximately 74 °C, the fueled hydrogen mass is only 3.3% less than the target value and the maximum energy saving at the refueling station accounts for 4.2 MJ per fueling. Additional benefits involve the cost reduction of the heat exchanger and increased reliability of the fueling process.

At the end, in order to maximize the hydrogen stored mass and minimize the extra volume and weight added to the tank, future research should focus on optimization studies that involve the heat transfer area and layer's thickness as the main variables. The PCM's properties can also be included in the optimization analysis to operate a comprehensive material selection in respect of the requirements identified above for the application of interest.

Acknowledgements

The authors acknowledge the Danish Energy Agency for financial support, our the industrial partner H2Logic, and all of the members of the Hyfill-Fast International Research Project for their collaboration.

Nomenclature

A_{hex}	heat transfer area, m^2
c_p	specific heat capacity at constant pressure, $J \cdot kg^{-1} \cdot K^{-1}$
k	phase change material's thermal conductivity, $W \cdot m^{-1} \cdot K^{-1}$
h	convective heat transfer coefficient, $W \cdot m^{-2} \cdot K^{-1}$
Q	cooling energy demand, J
$\dot{q}$	heat transfer rate for a single control volume, W
m	mass, kg
p	*pressure, bar*
R_{th}	thermal resistance, $K \cdot W^{-1}$
T	temperature, K or °C
t	time, s
V	volume, m^3
x	discretization step or location, m or mm

Greek symbols

ρ	density, $kg \cdot m^{-3}$
δ_1	value of the delta-function below the melting temperature, K or °C
δ_2	value of the delta-function above the melting temperature, K or °C
λ	specific latent heat of melting, $J \cdot kg^{-1}$

Subscripts

adiab	adiabatic conditions
in	inward
j	discrete index that refers to the discretized volumes
l	liquid phase
m	melting point
n	total number of discretized phase change material volumes
n_1	total number of discretized liner volumes
n_2	total number of discretized carbon fiber reinforced polymer volumes
out	outward
r	refers to the ratio between effective and liquid's thermal conductivity, $W \cdot m^{-1} \cdot K^{-1}$
r_1	refers to the ratio between effective and liquid's conductivity , $W \cdot m^{-1} \cdot K^{-1}$
r_2	refers to the ratio between effective and liquid's conductivity , $W \cdot m^{-1} \cdot K^{-1}$
s	solid phase
start	initial conditions
tot	total
½	refers to the half-thickness of the phase change material's layer
0	nominal conditions

Abbreviations

CFRP	carbon fiber reinforced polymer
CHG	compressed hydrogen gas
COP	Coefficient of performance
FCV	fuel cell vehicle
PCM	phase change material

References

[1] M. M. Farid, A. M. Khudhair, S. A. K. Razack, and S. Al-Hallaj, "A review on phase change energy storage: Materials and applications," *Energy Convers. Manag.*, vol. 45, pp. 1597–1615, 2004.

[2] M. Kenisarin and K. Mahkamov, "Solar energy storage using phase change materials," *Renew. Sustain. Energy Rev.*, vol. 11, no. 9, pp. 1913–1965, 2007.

[3] S. M. Shalaby, M. a. Bek, and a. a. El-Sebaii, "Solar dryers with PCM as energy storage medium: A review," *Renew. Sustain. Energy Rev.*, vol. 33, pp. 110–116, 2014.

[4] A. M. Khudhair and M. M. Farid, “A review on energy conservation in building applications with thermal storage by latent heat using phase change materials,” *Energy Convers. Manag.*, vol. 45, pp. 263–275, 2004.

[5] M. K. Choi, “Using Pre-melted Phase Change Material to Keep Payload Warm without Power for Hours in Space,” *CASI*, pp. 1–10, 2012.

[6] G. Tan and D. Zhao, “Study of a thermoelectric space cooling system integrated with phase change material,” *Appl. Therm. Eng.*, vol. 86, pp. 187–198, 2015.

[7] F. L. Tan, W. Shen, Jony, and S. C. Fok, “Thermal performance of PCM-cooled mobile phone,” *Proc. Electron. Packag. Technol. Conf. EPTC*, pp. 640–645, 2009.

[8] S. Mondal, “Phase change materials for smart textiles - An overview,” *Appl. Therm. Eng.*, vol. 28, no. 11–12, pp. 1536–1550, 2008.

[9] N. Sarier and E. Onder, “The manufacture of microencapsulated phase change materials suitable for the design of thermally enhanced fabrics,” *Thermochim. Acta*, vol. 452, no. 2, pp. 149–160, 2007.

[10] S. Garrier, B. Delhomme, P. de Rango, P. Marty, D. Fruchart, and S. Miraglia, “A new MgH2 tank concept using a phase-change material to store the heat of reaction,” *Int. J. Hydrogen Energy*, vol. 38, no. 23, pp. 9766–9771, Aug. 2013.

[11] S. J. Hynek and W. D. Fuller, “Stationary hydrogen storage using a phase change material,” *Hydrog. Energy Prog. XI*, vol. 2, pp. 1197–1202, 1996.

[12] A. Abhat, “Low temperature latent heat thermal energy storage: Heat storage materials,” *Sol. Energy*, vol. 30, no. 4, pp. 313–332, 1983.

[13] S. D. Sharma, H. Kitano, and K. Sagara, “Phase Change Materials for Low Temperature Solar Thermal Applications,” *Res. Rep. Fac. Eng. Mie Univ.*, vol. 29, pp. 31–64, 2004.

[14] I. Dincer and M. A. Rosen, *Thermal energy storage, Systems and Applications*. Chichester (England), 2002: John Wiley & Sons, 2002.

[15] G. A. Lane, “Low temperature heat storage with phase change materials,” *Int. J. Ambient Energy*, vol. 1, pp. 155–68, 1980.

[16] H. Kakiuchi, M. Yamayaki, M. Yabe, S. Chihara, Y. Terunuma, Y. Sakata, and T. Usami, “A study of erythritol as phase change material, 2nd Workshop of the IEA ECES IA Annex 10, Sofia (Bulgaria), 1998.,” in *2nd Workshop of the IEA ECES IA Annex 10*, 1998.

[17] A. Sari, A. Karaipekli, R. Eroğlu, and A. Biçer, "Erythritol Tetra Myristate and Erythritol Tetra Laurate as Novel Phase Change Materials for Low Temperature Thermal Energy Storage," *Energy Sources, Part A Recover. Util. Environ. Eff.*, vol. 35, no. April 2015, pp. 1285–1295, 2013.

[18] L. Royon, G. Guiffant, and P. Flaud, "Investigation of heat transfer in a polymeric phase change material for low level heat storage," *Energy Conversion and Management*, vol. 38. pp. 517–524, 1997.

[19] R. Naumann and H. H. Emons, "Results of thermal analysis for investigation of salt hydrates as latent heat-storage materials," *J. Therm. Anal.*, vol. 35, pp. 1009 – 1031, 1989.

[20] J. Heckenkamp and H. Baumann, "Latentwärmespeicher," *Sonderdruck aus Nachrichten 11*, pp. 1075–1081, 1997.

[21] R. B. Bird, W. E. Stewart, and E. N. Lightfoot, *Transport phenomena*, 2nd ed. New York (USA): John Wiley & Sons, 2002.

[22] F. Lindner, "Wärmespeicherung mit Salzen und Salzhydraten," *Ki Luft- und Kältetechnik*, vol. 10, pp. 462–467, 1996.

[23] T. Wada and H. Yoneno, "Studies on Salt Hydrates for Latent Heat Storage - Vii. the Relation Between Activation Process of Crystal Nucleation Catalysts for Sodium Acetate Trihydrate and Their Deactivation Temperatures," *Bull. Chem. Soc. Jpn.*, vol. 58, pp. 919–925, 1985.

[24] T. Wada and R. Yamamoto, "Studies on salt hydrate for latent heat storage. I. Crystal nucleation of sodium acetate trihydrate catalysed by tetrasodium pyrophosphate decahydrate," *Bull. Chem. Soc. Jpn.*, vol. 55, pp. 3603 – 3606, 1982.

[25] "International, Pilkington Solar, Survey of thermal storage for parabolic trough power plants," 2002.

[26] F. Graeter and J. Rheinländer, "Thermische Energiespeicherung mit Phasenwechsel im Bereich von 150 bis 400 °C," in *Proceedings of the Wärmespeicherung Workshop*, 2001.

[27] D. Heine and F. Heess, "Chemische uns physikalische Eigenschaften von Latentwärmespeichermaterialien für Solarkraftwerke," in *Proceedings of the 3rd International Solarforum,* 1980.

[28] B. Zalba, "Review on thermal energy storage with phase change: materials, heat transfer analysis and applications," *Appl. Therm. Eng.*, vol. 23, no. 3, pp. 251–283, 2003.

[29] Y. R. Tang, D. L. Gao, Y. F. Guo, S. Q. Wang, and T. L. Deng, "Supercooling and Phase Separation of Inorganic Salt Hydrates as PCMs," *Appl. Mech. Mater.*, vol. 71–78, pp. 2602–2605, 2011.

[30] S. Zuca, P. M. Pavel, and M. Constantinescu, "Study of one dimensional solidification with free convection in an infinite plate geometry," *Energy Convers. Manag.*, vol. 40, no. 3, pp. 261–271, 1999.

[31] M. Dimaano and A. Escoto, "Preliminary assessment of a mixture of capric and lauric acid for low-temperature thermal energy storage," *Energy*, vol. 23, pp. 421–7, 1998.

[32] D. Feldman, M. M. Shapiro, D. Banu, and C. J. Fuks, "Fatty acids and their mixtures as phase-change materials for thermal energy storage," *Sol. Energy Mater.*, vol. 18, no. 3–4, pp. 201–216, 1989.

[33] A. Hasan, "Phase change material energy storage system employing palmitic acid," *Sol. Energy*, vol. 52, no. 2, pp. 143–154, 1994.

[34] M. M. Farid, F. A. Hamad, and A.-A. M., "Phase change cool storage using dimethyl-sulfoxide," *Energy*, vol. 39, pp. 819–26, 1998.

[35] Hasnain S.M., "Review on sustainable thermal energy storage technologies, Part I: heat storage materials and techniques," *Energy Convers. Manag.*, vol. 39, no. 11, pp. 1127–1138, 1998.

[36] X. Py, R. Olives, and S. Mauran, "Paraffin/porous-graphite-matrix composite as a high and constant power thermal storage material," *Int. J. Heat Mass Transf.*, vol. 44, no. 14, pp. 2727–2737, 2001.

[37] P. B. Salunkhe and P. S. Shembekar, "A review on effect of phase change material encapsulation on the thermal performance of a system," *Renew. Sustain. Energy Rev.*, vol. 16, no. 8, pp. 5603–5616, 2012.

[38] H. H. Al-Kayiem and M. H. Alhamdo, "Thermal behavior of encapsulated phase change material energy storage," *J. Renew. Sustain. Energy*, vol. 4, no. 1, 2012.

[39] M. M. Farid and F. A. Hamad, "Melting and solidification in multi-dimensional geometry and presence of more than one interface," *Energy Convers. Manag.*, vol. 8, pp. 809–818, 1998.

[40] "Dymola, Dynamic Modeling Laboratory - User´s Manual," *Dynasim AB*.

[41] E. Rothuizen, W. Mérida, M. Rokni, and M. Wistoft-Ibsen, "Optimization of hydrogen vehicle refueling via dynamic simulation," *Int. J. Hydrogen Energy*, vol. 38, no. 11, pp. 4221–4231, Apr. 2013.

[42] F. P. Incropera, D. P. DeWitt, T. L. Bergman, and A. S. Lavine, *Fundamentals of Heat and Mass Transfer*, vol. 6th. John Wiley & Sons, 2007.

[43] E. Rothuizen and M. Rokni, "Optimization of the overall energy consumption in cascade fueling stations for hydrogen vehicles," *Int. J. Hydrogen Energy*, vol. 39, no. 1, pp. 582–592, 2014.

[44] Society of Automotive Engineers, "Fueling protocols for light duty gaseous hydrogen surface vehicle," *Tech. Inf. Rep. J2601*, 2010.

[45] M. Monde, P. Woodfield, T. Takano, and M. Kosaka, "Estimation of temperature change in practical hydrogen pressure tanks being filled at high pressures of 35 and 70 MPa," *Int. J. Hydrogen Energy*, vol. 37, no. 7, pp. 5723–5734, Apr. 2012.

[46] A. Elgowainy and K. Reddi, "Hydrogen Fueling Station Pre-Cooling Analysis," 2015 DOE Hydrogen and Fuel Cells Program. Annual Merit Review, June 2015. Available at: http://www.hydrogen.energy.gov/pdfs/review15/pd107_elgowainy_2015_o.pdf

[47] V. Canseco, Y. Anguy, J. J. Roa, and E. Palomo, "Structural and mechanical characterization of graphite foam/phase change material composites," *Carbon N. Y.*, vol. 74, pp. 266–281, 2014.

[48] S. Hong and D. R. Herling, "Aluminum Foam-Phase Change Material Composites as Heat Exchangers," *SAE Tech. Pap. Ser.*, no. 2007 World Congress Detroit, Michigan April 16–19, 2007, 2007.